Probing the Graphite Band Structure with Resonant Soft-X-Ray Fluorescence

J. A. Carlisle,[1] Eric L. Shirley,[1,*] E. A. Hudson,[1] L. J. Terminello,[1] T. A. Callcott,[2] J. J. Jia,[2] D. L. Ederer,[3] R. C. C. Perera,[4] and F. J. Himpsel[5]

[1]*Lawrence Livermore National Laboratory, Livermore, California 94551*
[2]*University of Tennessee, Knoxville, Tennessee 37996*
[3]*Tulane Unviersity, New Orleans, Louisiana 70118*
[4]*Lawrence Berkeley Laboratory, Berkeley, California 94720*
[5]*IBM Research Division, Thomas J. Watson Research Center, Yorktown Heights, New York 10598*
(Received 7 July 1994)

For incident photon energies near the core binding energy, inelastic x-ray scattering theory predicts a coherent absorption-emission process in which crystal momentum is conserved. Momentum conservation should manifest itself as dispersive features in fluorescence spectra. We report the detection of such features for the first time in graphite, and show that there exists a clear relationship between them and the graphite band structure. Our results demonstrate the potential of resonant soft-x-ray fluorescence for examining the momentum-resolved electronic structure of complex materials.

PACS numbers: 78.70.Dm, 71.35.+z, 71.55.Cn

As technologically relevant microelectronic materials become more complex, it becomes harder to characterize their bulk electronic structure. Because of the lack of atomic specificity of electron spectroscopies, techniques such as photoemission are often limited in elucidating the complex electronic properties of materials composed of several chemical elements. Buried heterojunction interfaces and materials sensitive to surface contamination are even more problematic to characterize, due to the short electron probing depth. Most insulating samples are impossible to characterize via photoemission due to charging effects.

Soft-x-ray fluorescence (SXF) spectroscopy using synchrotron radiation overcomes many of the disadvantages of electron spectroscopies [1]. SXF is *explicitly* a bulk-sensitive probe of the electronic structure. Photons penetrate many atomic layers deep into the material, as compared to a few atomic layers for electrons. Also, since core levels are involved in absorption and emission, SXF is element and angular momentum selective. SXF measures the local partial $(s, p, d, \ldots)$ density of states (DOS) for each constituent element of the material. The chief limitation of SXF has been the low yield for photon emission, particularly for light elements. However, third generation light sources, such as the Advanced Light Source (ALS), offer the high brightness that makes high-resolution SXF experiments practical.

In this Letter we present initial SXF experiments performed on the IBM/TENNESSEE/TULANE/LLNL/LBL beam line at the ALS. We have found clearly defined, dispersive features in the resonant SXF spectrum acquired from highly oriented, pyrolytic graphite (HOPG). The dependence of the dispersive features on the incident photon energy is related to the graphite band structure, as predicted by inelastic x-ray scattering theory. The results of this work suggest that resonant SXF can probe the element-specific momentum-resolved electronic structure of complex, multielement materials heretofore intractable using other techniques.

Recent experiments using SXF have examined the changes in the valence emission spectrum as the excitation energy ($h\nu_{\text{in}}$) is varied [2–8]. A valence emission spectrum results from transitions from valence band states to the core hole produced by $h\nu_{\text{in}}$. In the *nonresonant* energy regime, $h\nu_{\text{in}}$ is far above the Fermi level (E_F). The fluorescence spectrum resembles emission spectra acquired using energetic electrons, and is insensitive to $h\nu_{\text{in}}$. In the *resonant* energy regime, core electrons are excited by photons to unoccupied states just above E_F. The absorption and emission events are coupled, and this coupling manifests itself in several ways, depending in part on the degree of localization of the states above E_F in the material. In boron nitride, the resonant emission spectrum reflects the influence of an electron excited to a *localized,* excitonic state [2]. The combined influence of the localized electron and the core hole screens the valence electrons, resulting in a shift of the valence emission to lower photon energies. Resonant SXF experiments involving *delocalized* final states in graphite [3], Si [4], diamond [5,6], and Mg and Al oxides [7] have instead found intensity modulations in the emission spectrum as $h\nu_{\text{in}}$ is varied. The experiments on Si and diamond have been interpreted in terms of a crystal momentum conserving (**k**-conserving) absorption-emission process, which provides an energy loss mechanism analogous to resonant x-ray Raman scattering [5,6,8,9]. This theory of the **k**-conserving inelastic scattering process accounts for the observed modulations fairly well, but to date no *dispersive* emission features (also predicted by the theory) have been observed.

Resonant versus off-resonant fluorescence spectra that were measured from HOPG at the ALS are shown in Fig. 1. Figure 2(a) shows the experimental geometry used to acquire the spectra. The takeoff angle α for this data

 0031-9007/95/74(7)/1234(4)$06.00

was 35°, and the width of the excitation energy was approximately 0.3 eV. The uppermost spectrum is characteristic for the nonresonant case far above threshold ($h\nu_{in}$ = 400 eV). Peaks in the off-resonant spectrum derive primarily from flat regions in the band structure (such as around critical points), which are regions having a high DOS. The resonant spectra are shown below the nonresonant spectrum. Most of these spectra have a drastically different line shape compared to the nonresonant one. Instead of mere intensity fluctuations observed in other delocalized materials, most of the emission peaks appear to disperse. Their *emitted* photon energies ($h\nu_{out}$) change as $h\nu_{in}$ is varied from 284 to 287 eV. These dispersive peaks are highlighted by the dashed lines and are numbered 1–7 in Fig. 1. The changes in the emission spectrum are most dramatic when $h\nu_{in}$ is varied by just 0.5 eV, from 284.5 to 285 eV. The intensities of features 3 and 4 abruptly increase, while peaks 2 and 3 diminish substantially. Such large changes in the spectrum due to such small changes in $h\nu_{in}$ cannot be accounted for solely by simple intensity modulations, which have been explained in terms of sweeping through critical points in the Brillouin zone [5,6].

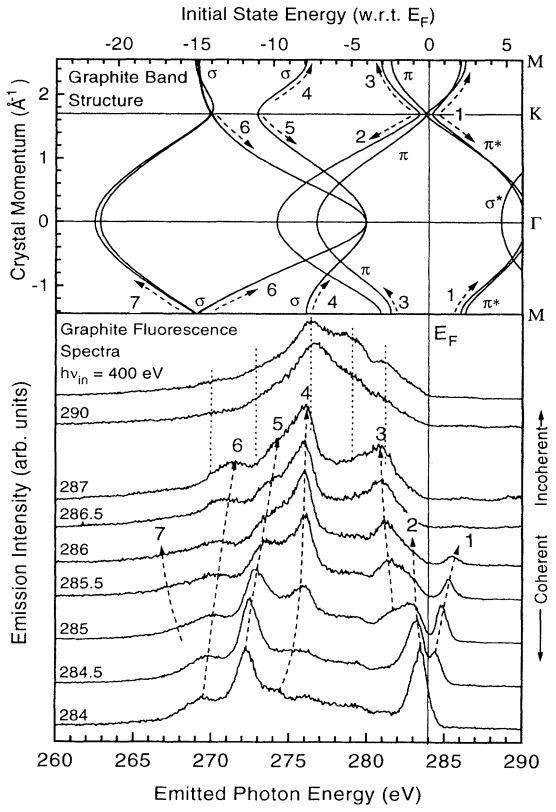

FIG. 1. Resonant and nonresonant fluorescence spectra from highly oriented pyrolytic graphite at incident energies $h\nu_{in}$. The upper panel displays the graphite band structure with the energy axis matched to the photon energy axis of the fluorescence data. The dispersive features labeled 1–7 in the resonant spectra are associated with the portions 1–7 of the graphite band structure indicated by dashed lines and arrows in the upper panel.

The $h\nu_{in}$ dependent emission features are the result of transitions from states with a well defined crystal momentum. The upper panel of Fig. 1 shows the band structure of graphite along the high symmetry directions as derived from a tight-binding parametrization of quasiparticle calculations [10]. The σ and π molecular orbitals give rise to the bands labeled in Fig. 1, and correspond to the different types of bonding (σ or π bonding) which arise between carbon atoms in the graphite sheets. In this figure the band structure has been rotated and the binding energy axis aligned to the lower panel's photon energy axis.

According to inelastic x-ray scattering theory, in the coherent absorption-emission process the energies of the incident and emitted photons are related by the expressions [5,6,8,9]

$$h\nu_{in} = E_c(\mathbf{k}_c) - E_{core}\,, \tag{1}$$

$$h\nu_{out} = E_v(\mathbf{k}_v) - E_{core}\,, \tag{2}$$

and

$$\mathbf{k}_v + \mathbf{q}_{in} = \mathbf{k}_c + \mathbf{q}_{out} = \mathbf{G}\,. \tag{3}$$

In these expressions, E_{core} is the C(1s) binding energy with respect to E_F. The variable $E_c(\mathbf{k}_c)$ [$E_v(\mathbf{k}_v)$] is the conduction band (valence band) binding energy, indexed to the crystal momentum vector $\mathbf{k}_c$ ($\mathbf{k}_v$), and $\mathbf{q}_{in}$ ($\mathbf{q}_{out}$) is

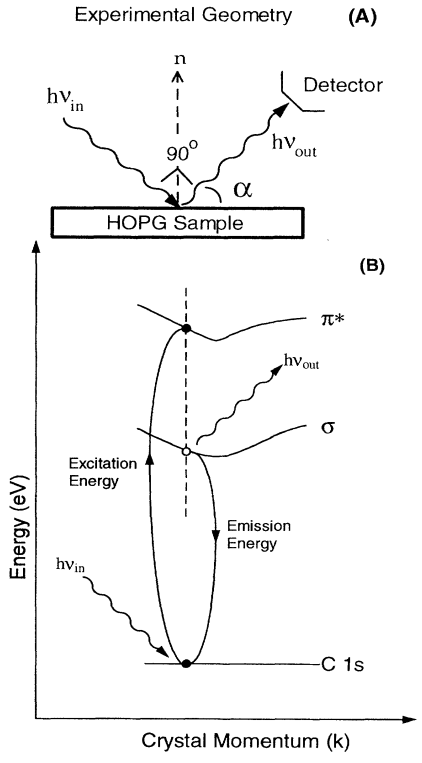

FIG. 2. (a) Experimental geometry used. α is the takeoff angle. (b) Schematic representation of coherent fluorescence. After the incident photon excites the core electron to the empty π^* band, only emission from occupied states with the same crystal momentum (vertical line) is allowed.

the momentum vector of the incident (emitted) photon. For most of this work $E_c(\mathbf{k}_c)$ corresponds to the π^* conduction band of graphite. If the photon momenta are neglected Eq. (3) becomes $\mathbf{k}_v = \mathbf{k}_c$ in the reduced zone.

Figure 2(b) shows schematically the coherent absorption-emission process as inferred from Eqs. (1)–(3). Control over $h\nu_{\text{in}}$ allows one to select the crystal momentum of the photoelectron's final state in the conduction band [through conservation of energy in Eq. (1)]. Thus by Eq. (2) the allowed transitions from occupied states fill the core hole and lie on a vertical line through the band structure having the same crystal momentum as the electron in the π^* conduction band. One may predict the dispersive behavior of the emission peaks graphically in Fig. 2(b) by constructing sets of vertical lines whose $\mathbf{k}$-values are determined by which $\mathbf{k}$-point in the π^* band the core electron is excited to by $h\nu_{\text{in}}$. The allowed transitions (along the high symmetry directions only) are determined by where the lines intersect the bands. The result of such an analysis leads in a straightforward way to the association of different portions of the graphite band structure in the upper panel of Fig. 1, which are labeled 1–7, with the emission features labeled 1–7 in the lower panel. Clearly, there is a correlation between the dispersive emission features and the σ and π bands of the HOPG band structure.

Our assignment of the emission features to the band structure in Fig. 1 is corroborated by two observations. First, the assignment explains in a simple way the sudden intensity increase of features 3 and 4 noted earlier. As $h\nu_{\text{in}}$ nears 286 eV, the core electron is excited to the M point in the Brillouin zone. At this point in k-space the bands are flat, so their densities of states are relatively high. M is a saddle point in both the π and π^* bands. Peaks 3 and 4 arise from transitions near this critical point, and are thus relatively enhanced as compared to features 2 and 5, which are due to transitions from points in k-space between Γ and K.

The angular dependence of the emission features also corroborates our assignment. This angular dependence is shown in detail in Fig. 3(a). By adjusting the takeoff angle α of the emitted photons, it is possible to differentiate between σ and π emission [3]. The π emission is derived from transitions from p_z states oriented perpendicular to the graphite plane. Emission from the σ bands is much more isotropic since they are derived in part from the p_x and p_y states oriented parallel to the surface. By adjusting the takeoff angle from near grazing ($\alpha = 25°$) to near normal ($\alpha = 70°$) in Fig. 3(a), we observed the intensities of features 2 and 3 drop significantly (almost to zero), as opposed to peaks 4–7, which were relatively unaffected. Since in our assignment the features 2–3 are due to π band emission, whereas features 4–7 are due to σ band emission, this takeoff angle dependence further supports our assignment.

The graphical procedure in Fig. 2(b) for predicting the dispersive behavior of the emission peaks is an approxi-

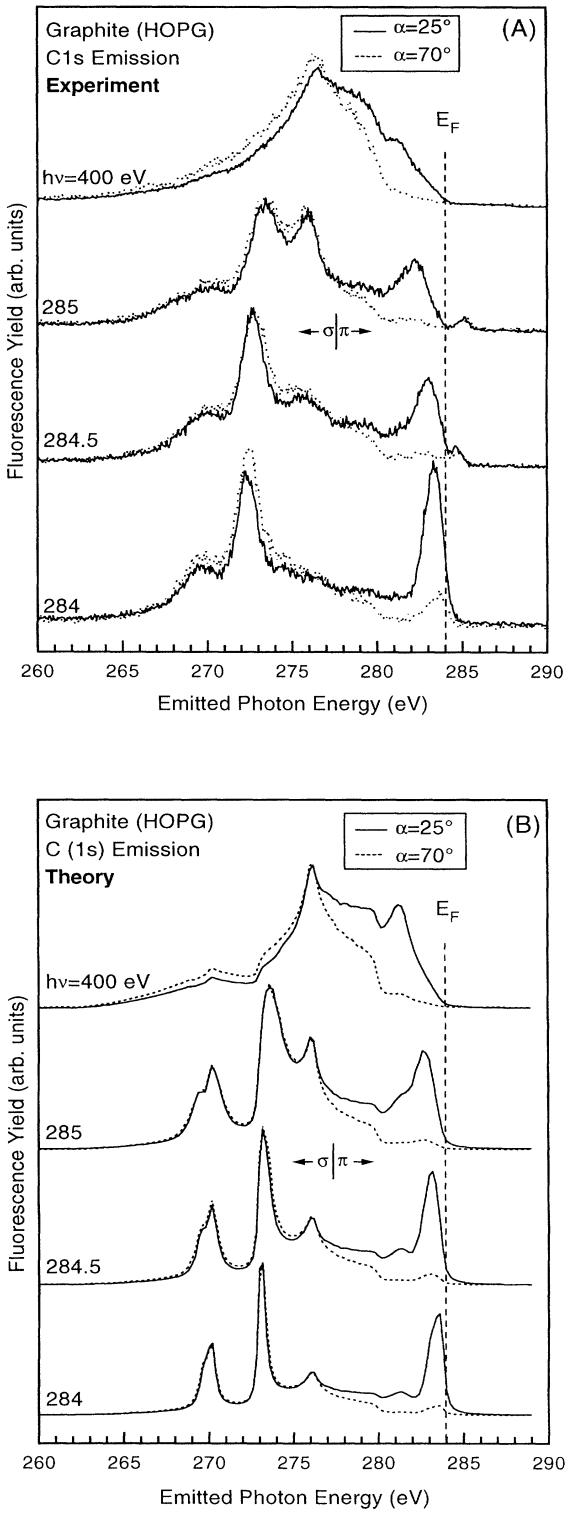

FIG. 3. (a) Resonant and nonresonant fluorescence spectra acquired using takeoff angles of $\alpha = 25°$ (lines) and $\alpha = 70°$ (dots). (b) Calculated emission spectra obtained assuming coherent absorption or emission as described in the text. A small fraction (0.2–0.4) of the incoherent spectrum has been added to the theoretical spectra.

mation. The photoexcited core electron is not constrained to portions of the zone along the high symmetry directions, but may be promoted to any portion of an isoenergy surface allowed by conservation of energy in Eq. (1). In fact, for $h\nu_{\text{in}} = 284$ eV, the core electron is excited to the Fermi surface. The isoenergy surfaces probed in this experiment are most similar to those imaged by an angle-resolved photoemission experiment which utilized a display-type analyzer [11]. The emission spectra in Fig. 1 have contributions from all points on these surfaces as well as their intersection with the high symmetry directions. A detailed test of our model for the coherent fluorescence thus requires a calculation of the spectra based on the inelastic x-ray scattering theory mentioned earlier. Such a comparison is given in Fig. 3, where we show experimental data acquired at two extreme takeoff angles in Fig. 3(a), whereas Fig. 3(b) shows theoretical spectra calculated under the same conditions as described below. As can be seen in Fig. 3, the agreement between theory and experiment is quite good.

Evaluation of the theoretical emission spectra shown in Fig. 3(b) amounts to a determination of the local density of states summed over the appropriate isoenergy surfaces. Equations (1)–(3) result from an evaluation of the resonant term in the Kramers-Heisenberg formula from the theory of inelastic scattering [5,6,8,9]:

$$\frac{d\sigma}{d\Omega} \propto \left| \sum_m \frac{\langle f|\,\mathbf{p}\cdot\mathbf{A}\,|m\rangle\langle m|\,\mathbf{p}\cdot\mathbf{A}\,|i\rangle}{E_m - E_i - h\nu_{\text{in}} - i\Gamma/2} \right|^2 . \qquad (4)$$

In this expression the initial state $|i\rangle$ is the ground state, whereas the final state $|f\rangle$ has an electron in the conduction band and a hole in the valence band. The intermediate states $|m\rangle$ have a C($1s$) core hole and an electron in the conduction band.

A particularly interesting aspect of the experimental spectra is the pronounced emission from the π bands. In the simplest theory of coherent fluorescence, copious emission by π states is forbidden: π and π^* states exhibit opposite phase relations regarding their amplitudes on the two carbon atoms in the graphene unit cell. Electric-quadrupole and other effects (such as the finite photon momenta) weakly allow π emission, while large emission seen in experiment could be due to inequivalence of these two carbon atoms in the presence of AB stacking. In our theory, we introduce such an inequivalence. Theoretical π-emission peak heights do not grow simply as the length of the isoenergy contour owing to including longer electron lifetimes near E_F, which achieves a behavior in the π-emission peak heights similar to that found in experiment.

To summarize, we have used high-resolution soft-x-ray fluorescence spectroscopy with synchrotron radiation at the ALS to probe the bulk electronic structure of highly oriented pyrolytic graphite. Dispersive features in the emission spectra have been clearly observed, and it has been shown that these dispersive features arise due to a coherent absorption-emission process in which momentum is conserved. Thus, by tuning the incident photon energy to place the core electron into unoccupied states in the conduction band with a well defined momentum, we are able to probe the band structure of a material. The local momentum-resolved electronic configuration on each constituent element of a more complex (possibly insulating) material may be characterized with this technique as well.

This work was supported by the Division of Materials Science, Office of Basic Energy Sciences, and performed under the auspices of the U.S. Department of Energy by Lawrence Livermore National Laboratory under Contract No. W-7405-ENG-48, by National Science Foundation Grants No. DMR-9017996 and No. DMR-9017997, by a Science Alliance Center for Excellence Grant from the University of Tennessee, and by the U.S. Department of Energy (DOE) Contract No. DE-AC05-84OR21400 with Oak Ridge National Laboratory. This work was performed at the Advanced Light Source, which is also supported by the Office of Basic Energy Sciences, U.S. Department of Energy, under Contract No. DE-AC03-76SF00098.

*Present address: National Institute of Standards and Technology, Gaithersburg, MD 20899

[1] See, for instance, D. L. Ederer, T. A. Callcott, and R. C. C. Perera, Synchrotron Radiat. News **7**, 29 (1994).

[2] W. L. O'Brien, J. Jia, Q.-Y. Dong, T. A. Callcott, K. E. Miyano, D. L. Ederer, D. R. Mueller, and C-C. Kao, Phys. Rev. Lett. **70**, 238 (1993).

[3] P. Skytt, P. Glans, D. C. Mancini, J.-H. Guo, N. Wassdahl, J. Nørdgren, and Y. Ma, Phys. Rev. B **50**, 10457 (1994).

[4] J-E. Rubensson, D. Mueller, R. Shuker, D. L. Ederer, C. H. Zhang, J. Jia, and T. A. Callcott, Phys. Rev. Lett. **64**, 1047 (1990); K. E. Miyano, D. L. Ederer, T. A. Callcott, W. L. O'Brien, J. J. Jia, L. Zhou, Q.-Y. Dong, Y. Ma, J. C. Woicik, and D. R. Mueller, Phys. Rev. B **48**, 1918 (1993).

[5] P. D. Johnson and Y. Ma, Phys. Rev. B **49**, 5024 (1994).

[6] Y. Ma, N. Wasshahl, P. Skytt, J. Guo, J. Nørdgren, P. D. Johnson, J.-E. Rubensson, T. Boske, W. Eberhardt, and S. D. Kevan, Phys. Rev. Lett. **69**, 2598 (1993), and references therein.

[7] W. L. O'Brien, J. Jia, Q.-Y. Dong, T. A. Callcott, D. R. Mueller, D. L. Ederer, and C.-C. Kao, Phys. Rev. B **47**, 15482 (1993).

[8] Y. Ma, Phys. Rev. B **49**, 5799 (1994).

[9] T. Aberg, Phys. Scr. **21**, 495 (1980); J. Tulkki and T. Aberg, J. Phys. B **15**, L435 (1982); J. Tulkki, Phys. Rev. A **27**, 3375 (1983).

[10] X. Zhu and S. G. Louie (unpublished); see also I. T. McGovern, W. Eberhardt, E. W. Plummer, and J. E. Fischer, Physica (Amsterdam) **99B**, 415 (1980); R. F. Willis, B. Feuerbacker, and B. Fitton, Phys. Rev. B **4**, 2441 (1971).

[11] A. Santoni, L. J. Terminello, F. J. Himpsel, and T. Takahashi, Appl. Phys. A **52**, 299 (1991).